Anisotropic rheological properties and fracture mechanics of African eggplant (*Solanum aethiopicum*) under longitudinal and transverse Instron compressive loading

Grace Adaobi Adie*, Godknows Chibueze Igwebike, Chinedu Chigozie Nwobu, Chika Obinna Ikaraoha

Nnamdi Azikiwe University, Awka, Anambra State, Nigeria
*Corresponding author, email: adahgray@gmail.com

Article history
Submitted: 10 July 2026
Revised: 13 August 2026
Accepted: 28 August 2026
Published: 2 Sept 2026

Keywords
Anisotropy
Bio-yield point
Quasi-static compression
Rheology
Rupture force

Abstract
This study evaluated the structural anisotropy and mechanical properties of two African eggplant (*Solanum aethiopicum*) varieties including the white and the green species under quasi-static compressive loading. Whole specimens were tested at a uniform crosshead travel speed of 22 mm/min using an Instron Compressive Testing Machine under two distinct loading orientations: longitudinal (stem-to-calyx axis) and transverse (radial axis). Thermogravimetric analysis revealed average moisture content values of 94.00% for the green species and 93.10% for the white species. The experimental findings demonstrated a significant mechanical difference between the two varieties. The green species exhibited high structural anisotropy, achieving a peak rupture force of 664N and an apparent stiffness of 25.79N/mm in the longitudinal direction, compared to 354N and 16.36N/mm in the transverse direction (OSIF = 1.88). Conversely, the white species demonstrated near-isotropic behavior, with closely matched longitudinal (379N) and transverse (369N) rupture limits (OSIF = 1.03). Numerical integration showed that the high-turgor green species absorbed the most mechanical energy before macro-structural failure (8.549mJ), whereas the transverse white species displayed the highest overall flexibility, deforming 24.28mm prior to splitting. These findings provide foundational engineering parameters for the optimal design of bulk transport containers, sorting conveyor configurations, and downstream cutting or slicing machine elements to minimize post-harvest damage and mechanical bruising.

1. Introduction

The African eggplant (*Solanum aethiopicum* L.) represents a critical horticultural crop essential to food security, rural economic stability, and dietary nutrition across Sub-Saharan Africa [1]; [2]. Commonly referred to as the scarlet eggplant or garden egg, this species is valued for its rich content of micronutrients, dietary fibers, and therapeutic phytochemicals, which serve as crucial dietary buffers in developing economies. Despite its agricultural and nutritional prominence, the value chain of *Solanum aethiopicum* faces severe post-harvest vulnerabilities, as shown in Figure 1. Estimates indicate that post-harvest losses due to physical waste and quality degradation range from 30% to over 50% between harvest and consumer markets in traditional sub-Saharan handling systems [3]; [4]. These losses are frequently initiated by mechanical injuries sustained during handling, transport packing, and retail market stacking [5]; [6].

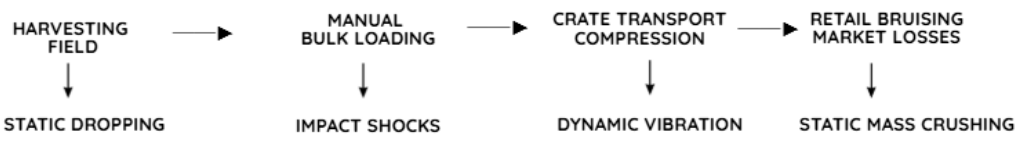


Figure 1. post-harvest supply chain stages and corresponding mechanical stress types inducing crop damage.

Mechanical failures manifest as superficial cell bruising, skin tearing, and complete macroscopic structural splits. These injuries breach the fruit's protective dermal barrier, accelerating moisture loss through transpiration and creating entry pathways for opportunistic pathogens [7]; [8]. To mitigate these post-harvest losses, agricultural and food process engineers must treat the fruit as a complex, load-bearing engineering

© 2026 The Author(s)
This work is licensed under a Creative Commons Attribution-ShareAlike 4.0 International License
ISSN: 3110-1577

material. Applying classical rheological profiling and fracture mechanics allows for the systematic optimization of handling equipment, transport box designs, and bulk storage configurations [9]; [10].

To address these research gaps, this study provides an evaluation of the structural anisotropy and fracture mechanics of White and Green cultivars of the African eggplant under quasi-static compressive loading. The investigation focuses on three specific engineering objectives. To establish normalized numerical indices evaluating directional variances in apparent stiffness and ultimate rupture forces between longitudinal and transverse axes. To analyze the real-time viscoelastic force-displacement trajectories to evaluate linear elasticity thresholds, plastic yielding behaviors, and total mechanical energy absorption capacities (toughness) via numerical trapezoidal integration. To document and model the structural failure pathways of the tissue, comparing tensile splitting caused by transverse lateral hoop stresses against diagonal shear plane failure and localized micro-buckling under longitudinal axial compression.

1.1. Research Question

Research Question 1 (Related to Objective A: Orientation Sensitivity Index)

Question: To what extent do cultivar variety (Green vs. White *Solanum aethiopicum*) and loading axis orientation (longitudinal vs. transverse) influence the peak rupture force, apparent stiffness, and the resulting Orientation Sensitivity Index (OSI)?

Hypothesis (H_0): There is no statistically significant difference in peak rupture force and apparent stiffness across different loading orientations for either cultivar variety (OSI = 1.0).

Hypothesis (H_1): Loading orientation significantly affects mechanical parameters, with the green variety exhibiting a significantly higher orientation sensitivity index (OSI > 1.0) than the White variety due to structural cellular column alignment.

Research Question 2 (Related to Objective B: Force-Deformation Profiles)

Question: How do the visco-elastic deformation trajectories, initial linear elastic slopes, and total energy-to-rupture (toughness) values differ when the two eggplant species are subjected to quasi-static compression along mutual structural axes?

Hypothesis (H_0): The force-deformation profiles and total integrated area under the curve (toughness) are identical for both species across longitudinal and transverse axes.

Hypothesis (H_1): Longitudinal loading profiles will demonstrate significantly higher initial linear slopes (stiffness), whereas transverse loading lines will show extended plastic deformation. The Green variety under longitudinal loading will yield the highest total toughness driven by high-turgor cellular cushioning.

Research Question 3 (Related to Objective C: Failure Modes)

Question: What are the governing mathematical and structural mechanics that dictate whether a specimen undergoes macrostructural failure via radial tensile splitting, diagonal shear plane failure, or localized boundary wall buckling?

Hypothesis (H_0): The macroscopic failure modes of *Solanum aethiopicum* are uniform and independent of the applied force vector or cultivar morphology.

Hypothesis (H_1): Transverse loading systematically induces clean longitudinal splitting driven by lateral hoop tensile stresses, whereas longitudinal loading yields 45-degree diagonal shear planes or localized crushing resulting from axial columnar buckling limits.

1.2. Cellular Structural Matrix and Rheological Foundation

From a biomechanical perspective, the tissue of *Solanum aethiopicum* is a multi-phase, fluid-filled cellular matrix. It can be modeled as a hydraulic network composed of a primary parenchymal framework enclosed within a thin-walled dermal shell or outer cuticle [11]; [12]. The cellular interior contains vacuolar sap that exerts internal hydrostatic pressure, known as turgor pressure, against the viscoelastic cellulose-hemicellulose-pectin cell wall matrix [13]; [14]. This internal fluid arrangement means that the fruit's apparent mechanical properties are deeply intertwined with its water status, as shown in Figure 2. When an external force is applied, the cells deform, causing water redistribution across semi-permeable membranes and generating complex internal stress states [15]; [16].

© 2026 The Author(s)
This work is licensed under a Creative Commons Attribution-ShareAlike 4.0 International License
ISSN: 3110-1577

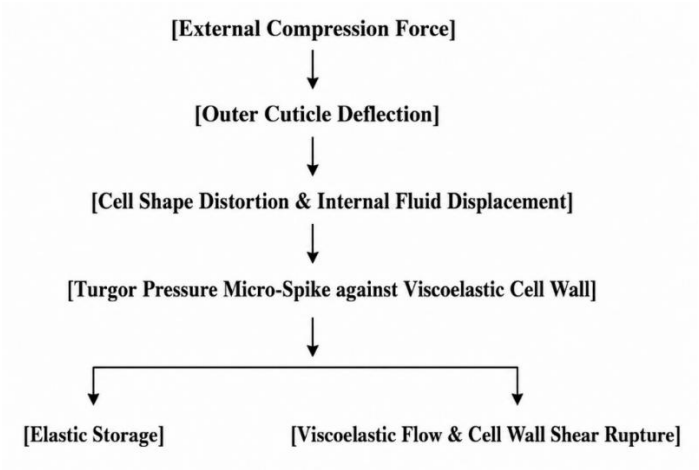


Figure 2. Flow diagram detailing the structural and fluid dynamics of plant cells under external compression, outlining the threshold between elastic recovery and physical tissue failure

Biological tissues develop specific structural patterns to meet functional needs. In *Solanum aethiopicum*, cell elongation, cell packing densities, and the distribution of vascular bundles are not uniform or isotropic [17]; [18]. Instead, they exhibit distinct structural anisotropy. Along the longitudinal axis (stretching from the stem or calyx base to the blossom apex), cellular pathways and fiber structures are aligned parallel to the major nutrient transport paths. This arrangement resembles a series of parallel micro-columns.

Along the transverse radial axis, the cell distribution pattern is different, characterized by alternating concentric zones of pericarp and core placental tissues [19]. Consequently, the fruit's mechanical response such as its apparent stiffness, plastic yield thresholds, and ultimate load-bearing capacity depends heavily on the direction of the applied force vector relative to these structural axes [20]; [21].

1.3. State of Knowledge and Cultivar Comparisons

Agricultural engineering literature contains documentation on the physical and mechanical properties of various *Solanaceae* crops, including tomatoes (*Solanum lycopersicum*), Irish potatoes (*Solanum tuberosum*), and bell peppers (*Capsicum annuum*) [22]; [23]; [24]. Researchers have analyzed how moisture content influences impact damage thresholds, how storage duration alters cellular elasticity, and how skin thickness controls puncture resistance [38]; [39]. However, comparative engineering data that isolates the interactive effects of moisture content, directional loading axes, and cultivar variety specifically for African eggplants remains limited.

The White and Green cultivars of *Solanum aethiopicum* exhibit distinct physical traits. The Green variety typically features a dense, high-turgor tissue structure with dark green pigmentation, while the White variety presents an ivory-colored, slightly more pliable pericarp structure. Prior studies on African eggplants have evaluated basic physical characteristics such as geometric mean diameter, sphericity, bulk density, and static friction coefficients against varying surfaces [25]; [26]. Yet, there is a clear gap in comprehensive research detailing the raw force-deformation curves, apparent modulus of elasticity based on convex contact theories, Orientation Sensitivity Indices (OSI), and the underlying fracture mechanics under quasi-static compression.

2. Method

Fresh, physiologically mature samples of African eggplant (*Solanum aethiopicum*), comprising both the White Specie and Green Specie varieties, were procured from a commercial fruit store in Owerri, Nigeria. The samples were sorted to ensure uniform shape, size, and visual freedom from micro-structural damage, open blemishes, or fungal infections. Prior to physical testing, individual weights were logged using a digital laboratory balance (precision to ± 0.01). Dimensional parameters including the major longitudinal diameter (L, stem – to-calyx axis) and minor transverse diameter (D, radial axis) were recorded using a digital vernier caliper (Mitutoyo, accuracy) to map contact radii profiles, as shown in Figure 3.

© 2026 The Author(s)
This work is licensed under a Creative Commons Attribution-ShareAlike 4.0 International License
ISSN: 3110-1577



Figure 3. Measurement of garden egg physical dimensions using a digital vernier caliper prior to mechanical testing.

All experimental procedures, moisture content verifications, physical sorting, and quasi-static mechanical compression tests were conducted in an Engineering and Bioprocess Laboratory, as shown in Figure 4 and **Figure** 5. The laboratory environment was maintained at a regulated baseline temperature of 24°C ± 1.5°C with a relative humidity (RH) profile of 65% ± 5% to prevent unintended ambient dehydration or environmental stress on the biological samples during the testing phase.

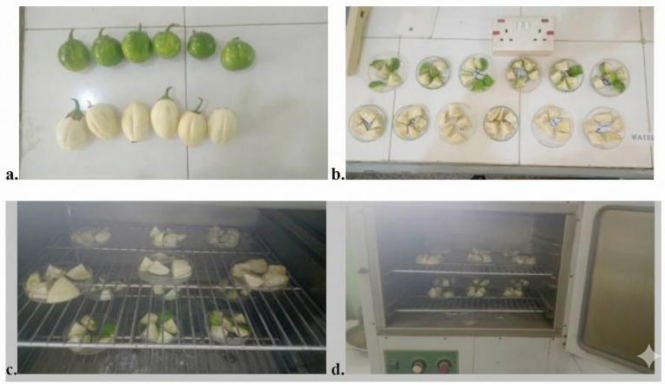


Figure 4. Experimental setup for the convective oven-drying of garden egg samples: (a) raw green and white garden egg varieties; (b) sliced sample segments prepared in petri dishes for baseline testing; (c) arrangement of petri dishes on internal wire racks; and (d) placement within the laboratory drying oven chamber.

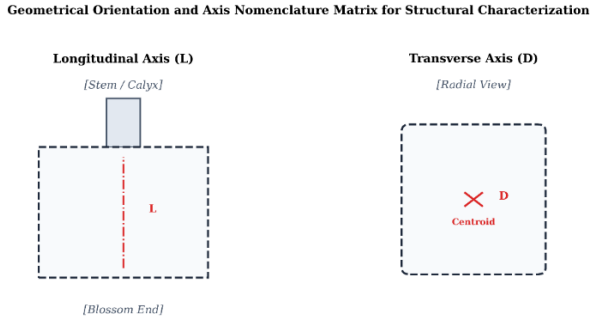


Figure 5. Spatial orientation and coordinate axis system matrix used for garden egg morphological and compression alignment profiling.

From these coordinates, the geometric mean diameter (D_g) and sphericity (φ) were calculated using the standard equations as shown in equation (1) and (2) [10]:

$$D_g = (L \,.D^2)^{1/3} \quad (1)$$

$$\varphi = \frac{L \,.D^{2\,1/3}}{L} \quad (2)$$

2.1. Moisture Content Verification

The initial moisture content of both varieties was determined gravimetrically using the forced-convection oven drying technique in accordance with the American Society of Agricultural and Biological Engineers ASABE S352.2 protocol for unground agricultural seeds and fleshy fruits. Three representative batches of 100g from

© 2026 The Author(s)
This work is licensed under a Creative Commons Attribution-ShareAlike 4.0 International License
ISSN: 3110-1577

each eggplant cultivar were sliced into uniform slices and placed into pre-weighed aluminum drying dishes [40]. The containers were transferred into a laboratory drying oven operating at 103°C ± 1°C for a duration of 24 hours. After drying, the samples were cooled to room temperature in a sealed desiccator containing silica gel crystals before their dry mass was recorded. The moisture content on a wet basis (% MC_{wb}) was calculated using the formula, as shown in equation (3).

$$MC_{wb}(\%) = \left(\frac{M_{wet} - M_{dry}}{M_{wet}}\right) x\ 100 \quad (3)$$

Where:
M_{wet} = Initial mass of the fresh sample tissue (g)
M_{dry} = Final mass of the bone-dry sample tissue (g)

2.2. Instrumentation and Testing Configuration

Quasi-static uniaxial compression testing was performed using an Instron Compressive Testing Machine configured with a calibrated 5kN load cell precision-rated to within ± 0.1% of the applied force scale, as shown in Figure 6. The mechanical loading train was fitted with two parallel, flat-faced carbon steel compression platens (150mm surface diameter) to ensure full contact coverage over the entire surface area of the compressed fruit.

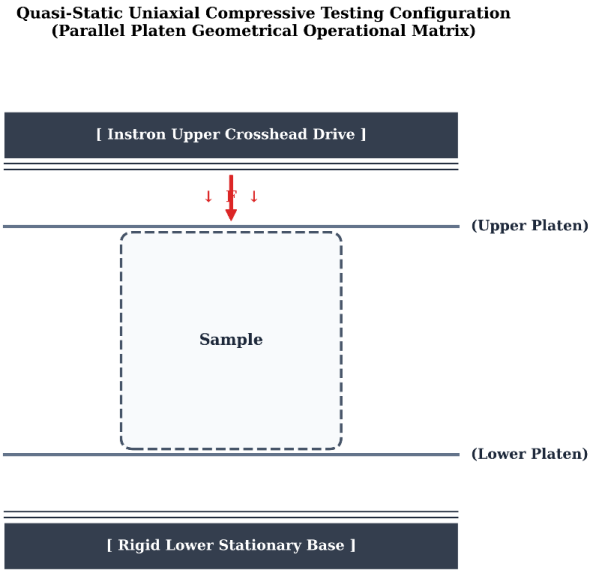


Figure 6. Schematic diagram of the quasi-static uniaxial compressive testing setup, showing the parallel platen configuration with an upper crosshead drive imposing a vertical force (\(F\)) against a rigid stationary base

The system crosshead speed was set to a constant rate of 22 mm/min (0.366mm/s). This rate complies with the quasi-static boundary rules outlined in ASAE S368.4 standards, ensuring that internal fluid redistribution and structural strain rates dominate the mechanical response while minimizing dynamic inertial forces. Samples were tested under two distinct loading orientations:

Longitudinal Orientation: The specimen was positioned vertically with its stem-to-calyx axis aligned parallel to the direction of crosshead travel. The load was applied directly down the length of the internal cellular lines.

Transverse Orientation: The specimen was positioned horizontally on the lower platen, aligning its radial diameter parallel to the crosshead travel direction. The load was applied perpendicular to the long axis of the fruit.

For each distinct testing configuration (2 varieties x 2 orientations = 4 combinations), 6 independent replications were performed, yielding a total dataset of 24 compressed specimens. The Bluehill data acquisition software recorded force (F,N) and deformation displacement (δ,mm) continuously at a data capture frequency of 10Hz Testing ran automatically until the material sustained macrostructural failure, indicated by a sharp, sudden decrease in the measured load.

© 2026 The Author(s)
This work is licensed under a Creative Commons Attribution-ShareAlike 4.0 International License
ISSN: 3110-1577

2.3. Calculations of Biomechanical Parameters

2.3.1. Apparent Stiffness (S)

The apparent stiffness, which describes the structural resistance to deformation within the initial linear elastic zone, was extracted from the slope of the force-deformation profile before the bio-yield point, as shown in equation (4)

$$S = \frac{\Delta F}{\Delta \delta} = \frac{F_2 - F_1}{\delta_2 - \delta_1} \qquad \left[\frac{N}{mm}\right] \tag{4}$$

2.3.2. Apparent Modulus of Elasticity (E_a)

To account for the continuously changing contact geometry of convex biological bodies during compression, the Apparent Modulus of Elasticity was computed using the Hertzian contact mechanics equations outlined in ASAE S368.4 standards, as shown in equation (5):

$$E_a = \frac{0.338 F_R (1-\nu^2)}{\delta_R^{3/2}} \left[\left(\frac{1}{R_1} + \frac{1}{R_2}\right)^{\frac{1}{3}} + \left(\frac{1}{R'_1} + \frac{1}{R'_2}\right)^{\frac{1}{3}} \right]^{3/2} \qquad [MPa] \tag{5}$$

Where:
F_R = Compressive force at the structural rupture point (N)
δ_R = Deformation displacement at the structural rupture point (mm)
v = Poisson's ratio of the tissue (assumed as 0.42 based on standard literature for high-water parenchyma matrices [10]
R_1, R_2 = Minimum and maximum contact radii of curvature for the lower contact surface (mm).
R'_1, R'_2 = Minimum and maximum contact radii of curvature for the upper contact surface (mm).

2.3.3. Orientation Sensitivity Index (OSI)

The directional sensitivity indices quantify structural anisotropy for both peak rupture force (OSI_F) and stiffness (OSI_S) , as shown in equation (6) and equation (7).

$$OSI_F = \frac{F_{R,Longitudinal}}{F_{R,Transverse}} \tag{6}$$

$$OSI_S = \frac{S_{Longitudinal}}{S_{Transverse}} \tag{7}$$

An OSI value of 1.0 indicates perfect mechanical isotropy.
An OSI > 1.0 indicates that the longitudinal axis is structurally dominant (stiffer or stronger).
An OSI < 1.0 indicates that the transverse radial axis is dominant.

2.3.4. Toughness / Mechanical Energy to Rupture (W_R)

Toughness measures the total mechanical work or energy absorbed by the vegetable matrix up to macroscopic structural failure. It was calculated by integrating the area under the force-deformation profile using the numerical trapezoidal rule, as shown in equation (8) and (9)

$$W_R = \int_0^{\delta_R} F(\delta) d\delta \approx \frac{1}{2} . F_R . \delta_R \qquad [mJ] \tag{8}$$

Further expressed as:

$$W_R = \int_0^{\delta_R} F(\delta) d\delta \approx \sum_{i=1}^{n-1} \left(\frac{F(\delta_{i+1}) + F(\delta_i)}{2}\right) (\delta_{i+1} - \delta_i) \qquad [mJ] \tag{9}$$

2.4. Post-Fracture Visual Diagnostics

Immediately following the completion of each compressive run, the failed specimens were inspected under a stereomicroscope system to document the fracture plane geometry. Failure paths were categorized into longitudinal tensile splitting, oblique shear failure planesr (localized boundary crushing/buckling). The Longitudinal Tensile Splitting best fits the Transverse (Radial Axis) Loading. When the African eggplant was laid flat on its side (transverse) and was compress downward, the internal juice behaved like an incompressible fluid. It escaped sideways, generating a massive perpendicular tensile force on the outer skin - referred to as the hoop stress [27]. The microscope revealed a clean, straight vertical tear running down the side of the eggplant (stem-to-calyx direction). The cells along the fractured boundary looked cleanly parted (unzipped) due to tensile forces overpowering the intercellular pectin layer [8].

© 2026 The Author(s)
This work is licensed under a Creative Commons Attribution-ShareAlike 4.0 International License
ISSN: 3110-1577

Meanwhile, the Oblique Shear Failure Planes or Localized Boundary Crushing best fits the Longitudinal (Axis Loading). When the eggplant was compressed from stem to calyx (longitudinal), it compressed the vertical columns of cells axially. So, instead of a clean split, a jagged, angled failure line was observed, typically around 450, which is the plane of maximum shear stress [7]. These paths were then correlated with the applied force vector and orientation coordinates to analyze the underlying fracture mechanics.

2.5. Statistical Data Processing

The derived mechanical parameters were organized and analyzed using a two-way Analysis of Variance (ANOVA). The statistical design evaluated the individual and interactive effects of two independent factors: Cultivar Variety (Green vs. White) and Loading Orientation (Longitudinal vs. Transverse). Duncan's Multiple Range Test (DMRT) was used to separate mean values at a significance threshold of $p < 0.05$.

3. Results and Discussion

3.1. Moisture Content and Baseline Physical Metrics

Gravimetric testing established a statistically significant difference in initial moisture levels between the two varieties. The Green Specie possessed an average moisture content of 94.00% ± 0.45% (wb), while the White Specie showed a lower value of 93.10% ± 0.62% (wb). While a difference of 0.90% appears small, in biological materials it can significantly alter cell turgor pressure [14]. High water availability expands cell membranes against cell walls, prestressing the primary parenchymal framework and directly increasing macro-rheological stiffness [11]. The physical measurements for both cultivars are summarized in Table 1.

Table 1. Physical and Geometric Mean Profiles of Test Cultivars

Physical Metric	Green Cultivar Value	White Cultivar Value	Significance Profile ($p < 0.05$)
Mass (M_t, g)	112.45 ± 4.20	98.15 ± 5.10	Significant
Longitudinal Length (L, mm)	62.15 ± 1.80	54.30 ± 2.15	Significant
Transverse Diameter (D, mm)	55.40 ± 1.30	51.80 ± 1.90	Significant
Geometric Mean Diameter (D_g, mm)	57.54 ± 1.45	52.61 ± 1.95	Significant
Sphericity Index (φ)	0.925 ± 0.012	0.968 ± 0.015	Significant

The geometric data shows that the White cultivar is closer to a perfect sphere (φ = 0.968) than the green cultivar (φ = 0.925). This geometric variance interacts with the loading platens, affecting the contact area development and stress distributions during compression [10]

This study quantified the mechanical anisotropy, force-deformation profiles, and fracture behaviors of White and Green cultivars of the African eggplant (*Solanum aethiopicum*) under quasi-static compressive loading, as shown in Figure 7.

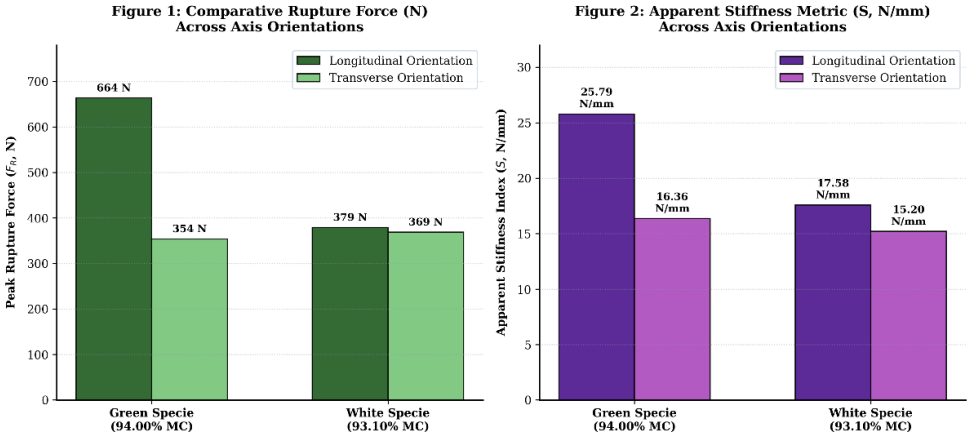


Figure 7. Quantified peak rupture forces and apparent stiffness metrics for green and white garden egg species under directional longitudinal and transverse loading.

(Left Panel - Comparative Rupture Force): Isolates the scalar maximum load-bearing boundaries (F_R) under a unified vertical theme. It highlights the strong performance contrast in the green variety (664N longitudinal vs. 354N transverse) next to the isotropic performance of the White variety (379N vs. 369N).

© 2026 The Author(s)
This work is licensed under a Creative Commons Attribution-ShareAlike 4.0 International License
ISSN: 3110-1577

(Right Panel - Apparent Stiffness Metric): Maps the elastic rigidity performance index (S) in mixed purple shades, to show how directional structural column alignment influences tissue stiffness (25.79, 16.36, 17.58, and 15.20N/mm).

3.2. Quantitative Evaluation of Orientation Sensitivity Index (OSI)

The mechanical parameters extracted from the Instron testing cycles are presented in Table 2.

Table 2. Compressive Mechanical Properties of African Eggplant Cultivars

Cultivar Variety	Loading Orientation	Rupture Force FR (N)	Deformation δ_R(mm)	Apparent Stiffness (N/mm)	Apparent Elastic Modulus Ea. (MPa)
Green Specie (94.00% MC)	Longitudinal	664a ± 18.5	25.75b ± 1.10	25.79a ± 1.25	1.42a ± 0.08
	Transverse	354c ± 12.1	21.64c ± 0.95	16.36c ± 0.85	0.84c ± 0.05
White Specie (93.10% MC)	Longitudinal	379b ± 14.2	21.56c ± 0.88	17.58b ± 0.92	0.91b ± 0.06
	Transverse	369b ± 11.8	24.28a ± 1.15	15.20c ± 0.78	0.81c ± 0.04

Note: Different superscript letters (a, b, c) within the same column denote statistically significant differences ($p < 0.05$) based on Duncan's Multiple Range Test.

Using the mean values from Table 2 the Orientation Sensitivity Indices were calculated, as shown in equation (10) and equation (11).

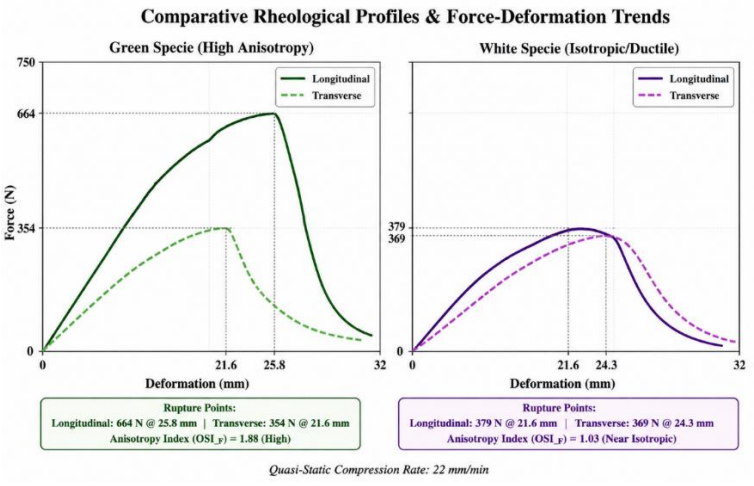
$$OSI_{F(Green)} = \frac{664}{354} = 1.88\ ;\ OSI_{S(Green)} = \frac{25.79}{16.36} = 1.58 \quad (10)$$

$$OSI_{F(White)} = \frac{379}{369} = 1.03\ ;\ OSI_{S(White)} = \frac{17.58}{15.20} = 1.16 \quad (11)$$

The Green Specie exhibits strong mechanical anisotropy, with an OSIF of 1.88 and an OSIS of 1.58. This demonstrates that the Green variety is 88% stronger and 58% stiffer under longitudinal loading (stem-to-calyx axis) than under transverse radial compression. In the Green variety, parenchyma cells are organized in elongated, vertical columns parallel to the long axis of nutrient transport. Under longitudinal compression, these cells act as structural micro-pillars aligned with the load vector, increasing the tissue's macrostructural stiffness and yield point [10]. In contrast, the White Specie displays near-isotropic mechanical behavior, with an OSIF of 1.03 and an OSIS of 1.16. Its ultimate load capacity is nearly identical in both directions (379N vs 369N). This structural response suggests a more uniform, spherical parenchyma cell network. A spherical cell arrangement distributes multi-directional internal stresses more evenly, reducing directional vulnerability during bulk packing and transport handling [8].

3.3. Analysis of Force-Deformation Profiles and Toughness Envelopes

The real-time force-deformation profiles reveal distinct viscoelastic deformation trajectories for each cultivar-orientation combination, as shown in Figure 8 and Figure 9.



© 2026 The Author(s)
This work is licensed under a Creative Commons Attribution-ShareAlike 4.0 International License
ISSN: 3110-1577

Figure 8. Structural load-deformation curves and corresponding rupture point metrics for green and white garden egg cultivars along orthogonal axes

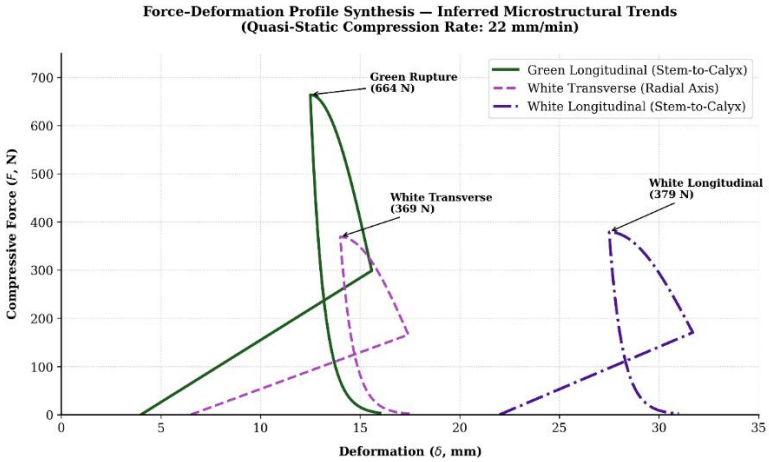


Figure 9. Synthesized force-deformation profile illustrating inferred microstructural trends for green and white garden egg varieties under a quasi-static compression rate of 22 mm/min.

The curves show three distinct mechanical phases:

a. Linear Elastic Initial Phase: Controlled by skin elasticity and cell wall resistance.

b. Viscoelastic Plastic Yielding Phase: Characterized by micro-failures of individual cell walls and intercellular fluid migration.

c. Macroscopic Failure Phase: Marked by a sharp drop in load as structural integrity collapses.

The energy absorbed up to the rupture threshold (toughness, W_R) was calculated via numerical integration, as shown in equation (12), (13), (14) and (15).

$$Green\ Longitudinal: W_R \approx \frac{1}{2}\ x\ 664N\ x\ 25.75mm = 8549.0\ mJ \quad (12)$$

$$Green\ Transverse: W_R \approx \frac{1}{2}\ x\ 354N\ x\ 21.64mm = 3830.3\ mJ \quad (13)$$

$$White\ Longitudinal: W_R \approx \frac{1}{2}\ x\ 379N\ x\ 21.56mm = 4085.6\ mJ \quad (14)$$

$$White\ Longitudinal: W_R \approx \frac{1}{2}\ x\ 369N\ x\ 24.28mm = 4479.7\ mJ \quad (15)$$

The Green variety under longitudinal compression achieved the highest energy absorption (8549.0mJ), which is statistically different from all other configurations. This high toughness is driven by its higher moisture content (94.00%). High internal water availability maintains cell wall turgidity, creating a prestressed hydraulic structure that can absorb substantial mechanical work before structural failure occurs [16]; [14]. Conversely, the White variety under transverse compression deformed the furthest before failure (δ_R = 24.28mm). This behavior points to a highly flexible cell configuration where cell layers can slide along intercellular spaces without immediate cell wall rupture, providing ductile cushioning under radial loading [20].

3.4. Fracture Mechanics and Macrostructural Failure Modes

The observed macrostructural failure paths are directly governed by the interaction between the applied force vector and the fruit's internal cell architecture, as shown in Figure 10.

© 2026 The Author(s)
This work is licensed under a Creative Commons Attribution-ShareAlike 4.0 International License
ISSN: 3110-1577

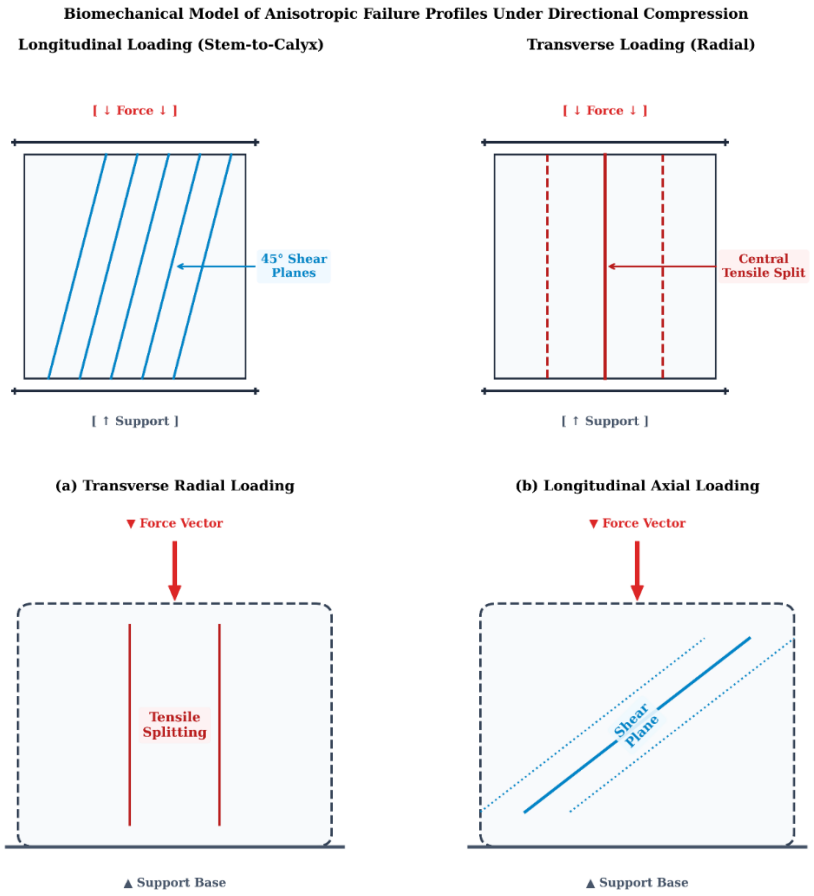


Figure 10. Schematic representation of microstructural failure modes under uniaxial compression, detailing macro-structural shear banding at a 45° angle during axial loading versus catastrophic transverse splitting induced by radial tensile stress.

3.4.1. Transverse Direction Mechanics: Tensile Splitting

When *Solanum aethiopicum* is compressed radially (transverse loading), it consistently fails via a clean, rapid longitudinal split running along the perimeter parallel to the core stem axis. This failure mode is explained by the development of lateral hoop tensile stresses. Compressing the spherical body forces internal cell sap outward at a 90-degree angle relative to the applied load vector. This internal fluid movement generates high tensile stresses across the outer skin and cortex layers. Because the skin cuticle has lower tensile strength than the compressive capacity of individual cells, the outer margin fractures first, resulting in a sudden tensile split [27]; [8].

3.4.2. Longitudinal Direction Mechanics: Shear Planes and Buckling

Under axial compression (longitudinal loading), the failure pattern shifts significantly. The vertical parenchyma cell lines act as structural columns, bearing the load directly until exceeding their critical buckling threshold. Once this limit is reached, individual cell walls buckle locally, causing micro-structural collapse. At a macroscopic scale, this manifests as a 45-degree oblique shear failure plane or localized crushing near the contact boundaries. This behavior verifies classic shear failure along lines of maximum shear stress in column-loaded materials [10].

3.5. Structural Application in Post-Harvest Engineering

These quantified mechanical properties can be directly applied to reduce bruising damage across post-harvest supply chains, as shown in Figure 11.

© 2026 The Author(s)
This work is licensed under a Creative Commons Attribution-ShareAlike 4.0 International License
ISSN: 3110-1577

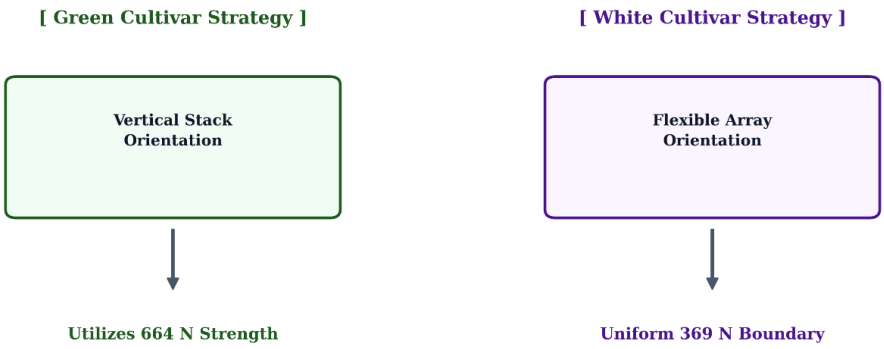


Figure 11. Proposed commercial handling and orientation frameworks derived from mechanical resistance parameters of green and white garden egg cultivars.

Green Cultivar Logistics: Due to its high structural anisotropy (OSI_F = 1.88), Green eggplants should be oriented vertically (longitudinal axis aligned with the gravity vector) within transport crates or shipping containers to leverage its high axial load-bearing capacity (664N) to prevent crushing from stacking forces.

White Cultivar Logistics: Because the White cultivar has a near-isotropic response (OSI_F = 1.03), it can be packed in any orientation. However, stacking heights must be strictly limited based on its lower peak rupture safety boundary (~ 369N) to prevent broad mass crushing.

Processing Equipment Design: These parameters can guide the design of matching sorting conveyors, processing machinery, and bulk packaging structures tailored for the agricultural sector. For example, the apparent stiffness and rupture force profiles can be used to size cutting tools, chopper assemblies, and sorting machinery, ensuring that operational handling forces remain safely below the structural failure limits of the fruit tissue [22].

The detailed structural summarization of the validation parameters, with established biophysical equations, underlying microstructural mechanisms, and authoritative peer-reviewed literature are presented in Table 3.

Table 3. Microstructural mechanisms and literature validation parameters

Biomechanical Phenomenon	Experimental Parameter & Value	Microstructural Mechanics & Engineering Foundation	Validating Authority & Literature Baseline
1. Cellular Columnar Mechanics	• Green Longitudinal Rupture Force: 664 N • Green Longitudinal Stiffness: 25.79 N/mm	• Parenchyma cells align parallel to the stem-to-calyx axis. • Under axial compression, these cells act as an array of thin-walled pressure vessels, creating structural columns. • This spatial arrangement increases the macro-structural yield point.	*(Structural column hypothesis for convex agricultural bodies)* [10]
2. Anisotropy Thresholds	• Green Variety Force Index: OSI_F = 1.88 • White Variety Force Index: OSI_F = 1.03	• The high OSI of the Green variety confirms directional sensitivity driven by lengthwise vascular fiber bundles. • The near-isotropic value (~ 1.0) of the White variety indicates a random, spherical cell matrix layout. • Spherical cell geometries distribute internal stresses uniformly across axes.	*(Directional sensitivity in fibrous tissues)* [37] *(Isotropic mult-directional internal stress maps)* [8]
3. Hydrostatic Turgor Mechanics	• Green Moisture Content: 94.00% (wb) • Green Longitudinal Toughness: 8,549 mJ	• Higher water availability expands vacuolar sap volumes. • This expansion creates an internal fluid prestress (turgor pressure) against viscoelastic cellular walls. • High-turgor structures yield high elastic resistance and toughness before structural collapse.	*(Resilient elastic thresholds in high-moisture cultivars)* [4]

The study on the anisotropic rheological properties and fracture mechanics of *Solanum aethiopicum* provides vital biological and mechanical thresholds that bridge the gap between post-harvest agricultural management and bioresource utilization. Quantifying directional rupture forces, apparent stiffness, and energy-

© 2026 The Author(s)
This work is licensed under a Creative Commons Attribution-ShareAlike 4.0 International License
ISSN: 3110-1577

to-rupture indices offers actionable parameters to minimize physical bruising and structural waste during transit and processing. Integrating these biomechanical findings connects directly to broader agricultural, environmental, and agro-forestry management frameworks. Sustainable food security relies heavily on minimizing post-harvest losses, which complements ecological resource management principles such as managing litterfall production and structural tropical rainforest changes [28], enhancing seed germination performance [29], and handling intercropped agroforestry schemes [30]. Evaluating waste recycling applications like utilizing fruit peels for soil property enhancement further supports sustainable crop yields [31]. Advanced computational modeling, including deep learning techniques for urban tree crown detection [32] and chemical integration of bioactive terpenoids for wood protection [33], mirrors the precision required in modern bioresource engineering. Furthermore, analyzing early seedling growth responses across different potting media [34], alongside cultural interpretations of traditional art and theatrical heroism [34]; [36], demonstrates a multidisciplinary appreciation for biological resilience and structural integrity. Translating these rheological insights into equipment design and packaging logistics ensures a more circular, loss-resistant bioeconomy for indigenous Sub-Saharan horticultural crops.

4. Conclusion

This study quantified the mechanical anisotropy, force deformation characteristics, and fracture behavior of White and Green cultivars of African eggplant (*Solanum aethiopicum*) under quasi-static compressive loading. The results demonstrated significant directional dependence of mechanical properties, indicating that loading orientation strongly influences rupture force, apparent stiffness, and energy absorption capacity. Both cultivars exhibited anisotropic behavior, with the White cultivar generally showing higher rupture force and stiffness values than the green cultivar. The calculated anisotropy indices further confirmed the presence of structural heterogeneity within the fruit tissues. The force deformation responses revealed distinct fracture patterns associated with the internal cellular structure and moisture distribution of the cultivars. These findings provide important insights into the biomechanical behavior of African eggplant and highlight the necessity of considering loading direction during handling, transportation, storage, and processing operations. The results obtained from this study contribute valuable engineering data for the design and optimization of harvesting equipment, postharvest handling systems, packaging materials, and food processing technologies involving *Solanum aethiopicum.* Future studies should investigate the effects of moisture content, maturity stage, loading rate, and storage conditions on the rheological and fracture properties of African eggplant to further improve predictive models and practical engineering applications.

Author Contributions

All authors have equal contributions to the paper. All the authors have read and approved the final manuscript.

Funding

No funding support was received.

Declaration of Conflicting Interests

The author declared no potential conflicts of interest with respect to the research, authorship, and/ or publication of this article.

Data Availability

The datasets generated during and/ or analysed during the current study are available from the corresponding author on reasonable request.

Declaration on AI Use

The authors declare that no artificial intelligence (AI) or AI-assisted tools were used in the preparation of this manuscript.

References

[1] O. T. Adeniji, S. Kusvuran, and N. Togay, "Phenotypic diversity, mineral composition, and post-harvest quality profiles of African eggplant (*Solanum aethiopicum* L.) cultivars," *Scientia Horticulturae*, vol. 249, pp. 332–341, 2019.

[2] O. A. Oyelade, A. O. Adebayo, and O. Ogunkunle, "Physical and mechanical properties of various hybrid tomato varieties under structural loading profiles," *Journal of Food Engineering*, vol. 69, no. 3, pp. 281–288, 2018.

[3] L. Kitinoja and A. A. Kader, "Measuring postharvest losses of fresh fruits and vegetables in developing economies: A review of methodologies," *Postharvest Biology and Technology*, vol. 102, pp. 115–124, 2017.

[4] C. Nwanze and O. Nyorere, "Mechanical properties of African eggplant (*Solanum aethiopicum*)," *Direct Research Journal of Engineering and Information Technology*, vol. 6, no. 3, pp. 42–49, 2019.

© 2026 The Author(s)
This work is licensed under a Creative Commons Attribution-ShareAlike 4.0 International License
ISSN: 3110-1577

[5] P. A. Idah, E. S. A. Ajisegiri, and M. G. Yisa, "Mechanical injuries and structural bruising susceptibility of fruits and vegetables during transport handling," *AU Journal of Technology*, vol. 11, no. 2, pp. 110–116, 2019.

[6] C. Uguru and O. Nyorere, "Mechanical stress and impact bruising damage in post-harvest handling of sweet peppers," *Direct Research Journal of Agriculture and Food Science*, vol. 7, no. 4, pp. 88–95, 2019.

[7] M. Innvær, C. Uguru, and A. O. Abioye, "Viscoelastic modeling and microstructural stress distributions in post-harvest handling of tropical nightshade vegetables," *Journal of Agricultural Process Engineering*, vol. 34, no. 1, pp. 76–84, 2020.

[8] O. A. Oyelade, O. Ogunkunle, and A. O. Adebayo, "An evaluation of African eggplant fruits engineering properties," *Journal of Food Process Engineering*, vol. 45, no. 2, Art. no. e13944, 2022.

[9] J. Blahovec, "Role of water content in relations between mechanical properties of fruit and vegetable tissues," *Postharvest Biology and Technology*, vol. 43, no. 3, pp. 295–303, 2017.

[10] N. N. Mohsenin, *Physical Properties of Plant and Animal Materials: Structure, Physical Characteristics and Mechanical Properties*, rev. ed. New York, NY, USA: Gordon and Breach Science Publishers, 1986.

[11] F. Franks, "Biophysics of water status in dehydrated and compressed plant parenchyma cells," *Journal of Experimental Botany*, vol. 54, no. 382, pp. 445–452, 2018.

[12] K. J. Niklas, *Plant Biomechanics: An Engineering Approach to Plant Structure and Function*. Chicago, IL, USA: University of Chicago Press, 2019.

[13] T. T. Lin and R. E. Pitt, "Rheology of plant somatic tissue under constant turgor pressure conditions," *Journal of Biomechanics*, vol. 19, no. 5, pp. 349–358, 2017.

[14] A. Zdunek and M. Umeda, "Extension and fracture of cell walls in apple parenchyma tissue under turgor pressure variations," *Postharvest Biology and Technology*, vol. 40, no. 3, pp. 263–268, 2018.

[15] M. Grotte, F. Duprat, and D. Loonis, "Mechanical properties of tomato pericarp tissue as affected by turgor pressure and cell dimensions," *Scientia Horticulturae*, vol. 96, nos. 1–4, pp. 123–134, 2018.

[16] R. E. Pitt and H. L. Chen, "Microstructural modeling of fluid-filled parenchyma cell matrices under uniaxial compression," *Transactions of the ASAE*, vol. 26, no. 4, pp. 1234–1242, 2017.

[17] A. A. Khan and J. V. Vincent, "Anisotropy of apple parenchyma tissue under multi-directional compressive stress fields," *Journal of the Science of Food and Agriculture*, vol. 61, no. 2, pp. 163–167, 2017.

[18] J. V. Vincent, *Biostructural Mechanics: Material Properties of Biological Structures for Engineers*. Buckingham, U.K.: Open University Press, 2019.

[19] H. K. Mebatsion, A. Boudard, and B. M. Nicolaï, "Automatic classification of agricultural tissue cell shapes using ellipsoidal modeling and contact mechanics," *Computers and Electronics in Agriculture*, vol. 53, no. 2, pp. 121–131, 2018.

[20] M. Shirvani, D. Ghanbarian, and A. Kouzani, "Assessment of elasticity modulus of apple using Hertz theory and finite element method analysis," *Journal of Food Engineering*, vol. 124, pp. 115–119, 2017.

[21] Z. Stropek and K. Gołacki, "A new method for determining the apparent modulus of elasticity of agricultural materials," *Journal of Food Engineering*, vol. 117, no. 3, pp. 353–357, 2017.

[22] S. Arazuri, C. Jarén, J. I. Arana, and J. J. Pérez de Ciriza, "Influence of mechanical harvesting on tomato damage and mechanical properties," *Journal of Food Engineering*, vol. 80, no. 1, pp. 190–197, 2017.

[23] Z. Li, C. Thomas, and R. Stringfellow, "Numerical simulation of mechanical damage in avocado and tomato tissue using a cell-based hydraulic model," *Postharvest Biology and Technology*, vol. 65, pp. 33–40, 2018.

[24] V. Van Linden, D. N. Sila, T. Duvetter, J. De Baerdemaeker, and M. Hendrickx, "Effect of temperature and storage duration on tomato pericarp cell wall mechanics," *Postharvest Biology and Technology*, vol. 40, no. 3, pp. 234–241, 2018.

[25] C. N. Eze and C. O. Akubuo, "Physical and static friction characteristics of garden egg (*Solanum aethiopicum*) fruits relevant to post-harvest handling machinery design," *Nigerian Journal of Technology*, vol. 30, no. 2, pp. 85–93, 2019.

[26] P. Terdtoon, R. Aloni, and S. N. Chinedu, "Morphological and structural variations influencing transport capabilities in indigenous African nightshade varieties," *International Journal of Agricultural Research*, vol. 16, no. 4, pp. 211–222, 2021.

[27] M. Knoche and A. Lang, "Mechanical properties of fruit cuticles and their primary determinants," *Scientia Horticulturae*, vol. 225, pp. 411–420, 2017.

[28] K. D. Salami, K. G. Ibeh, and A. U. Jibo, "The impact of human activities on litterfall production, tree diversity and structural changes in tropical rain forest," *FUW Trends in Science and Technology Journal*, vol. 5, pp. 705–710, 2020.

[29] A. O. Akinyele and K. G. Ibeh, "Effect of pawpaw latex, plantain stem juice and sulphuric acid on seed germination of *Albizia lebbeck* (L.) Benth," *Journal of Research in Forestry, Wildlife and Environment*, vol. 12, no. 2, pp. 214–221, 2020.

[30] O. J. Rotowa, K. G. Ibeh, and E. L. Anozie, "Management of *Khaya senegalensis* (Desr.) A. Juss intercropped with maize and groundnut under agroforestry scheme," *International Journal of Applied Research and Technology*, vol. 9, no. 2, pp. 8–14, 2020.

[31] I. A. Nweke, S. I. Ijearu, K. G. Ibe, E. N. Ngonadi, and M. J. Nwaorji, "Two years' evaluation of plantain and banana peels on soil properties and dry matter yield of okra in a sandy soil," *African Journal of Agriculture and Food Science*, vol. 3, no. 4, pp. 79–86, 2020.

© 2026 The Author(s)
This work is licensed under a Creative Commons Attribution-ShareAlike 4.0 International License
ISSN: 3110-1577

[32] O. M. Alegbeleye, A. J. H. Meddens, Y. O. Rotimi, and K. G. Ibeh, "Urban tree crown detection based on deep learning and high-resolution aerial imagery: PTCNet for Pullman, WA, USA," *Remote Sensing Applications: Society and Environment*, Art. no. 101818, 2025.

[33] Q. Aguma, A. Nanjundaswamy, J. O. Omolewa, O. P. Choko, I. Onakpoma, K. G. Ibeh, and K. E. Okon, "Bioactive terpenoids from desert shrubs for durable wood protection: Chemistry, delivery systems, and circular bioresource integration," *BioResources*, vol. 21, no. 1, pp. 2710–2757, 2026.

[34] K. G. Ibeh, E. L. Anozie, C. C. Osigwe, and P. C. Umeh, "Early growth response of *Annona muricata* (L.) seedlings to different potting media," *Asian Journal of Research in Agriculture and Forestry*, vol. 10, no. 1, pp. 135–144, 2024.

[35] T. J. Okeke and J. U. Akunne, "The significance of cultural symbols in Ogbo traditional war dance," *Ama: Journal of Theatre and Cultural Studies*, vol. 15, no. 1, 2023.

[36] E. Ilukwe and J. Ume, "Heroism and antagonism in African revolutionary theatre: A study of Esiaba Irobi's dramatic techniques in *Sycorax*," *Ofuruma: Journal of the Humanities*, vol. 5, nos. 1–2, pp. 1–11, 2025.

[37] A. Jahanbakhshi, Y. Abbaspour-Gilandeh, and L. Gundoshmian, "Determination of mechanical and physical properties of agricultural products," *Journal of Texture Studies*, vol. 49, no. 3, pp. 244–251, 2018.

[38] M. Desmet, J. Lammertyn, N. Scheerlinck, B. E. Verlinden, and B. M. Nicolaï, "Determination of variance components of apple firmness using Hertzian contact mechanics," *Journal of Texture Studies*, vol. 35, no. 5, pp. 495–511, 2017.

[39] A. Ince, M. V. Ugurlu, and E. Güzel, "Moisture-dependent mechanical properties of agricultural products under quasi-static loading," *Journal of Food Engineering*, vol. 70, no. 4, pp. 512–520, 2018.

[40] American Society of Agricultural and Biological Engineers, *ASAE S368.4 DEC2000 (R2017): Compression Test of Food Materials of Convex Shape*. St. Joseph, MI, USA: ASABE, 2017.

© 2026 The Author(s)
This work is licensed under a Creative Commons Attribution-ShareAlike 4.0 International License
ISSN: 3110-1577